Temperature tuning from direct to inverted bistable electroluminescence in resonant tunneling diodes

F. Hartmann,[1] A. Pfenning,[1] M. Rebello Sousa Dias,[2,3] F. Langer,[1] S. Höfling,[1,4] M. Kamp,[1] L. Worschech,[1] L. K. Castelano,[2] G. E. Marques,[2] and V. Lopez-Richard[2]

[1] *Technische Physik and Wilhelm Conrad Röntgen Research Center for Complex Material Systems, Physikalisches Institut, Universität Würzburg, Am Hubland, D-97074 Würzburg, Germany*
[2] *Departamento de Física, Universidade Federal de São Carlos, 13565-905 São Carlos, SP, Brazil*
[3] *Institute for Research in Electronics and Applied Physics, University of Maryland, College Park, Maryland 20742, United States*
[4] *SUPA, School of Physics and Astronomy, University of St Andrews, St Andrews, KY16 9SS, United Kingdom*

(Dated: September 15, 2017)

We study the electroluminescence (EL) emission of purely n-doped resonant tunneling diodes in a wide temperature range. The paper demonstrates that the EL originates from impact ionization and radiative recombination in the extended collector region of the tunneling device. Bistable current-voltage response and EL are detected and their respective high and low states are tuned under varying temperature. The inversion bistability of the EL intensity can be switched from direct to inverted with respect to the tunneling current and the optical on/off ratio can be enhanced with increasing temperature. One order of magnitude amplification of the optical on/off ratio can be attained compared to the electrical one. Our observation can be explained by an interplay of moderate peak-to-valley current ratios, large resonance voltages, and electron energy loss mechanisms and thus could be applied as an alternative route towards optoelectronic applications of tunneling devices.

PACS numbers: 78.60.Fi,72.20.Jv,72.10.Di,68.65.-k

I. INTRODUCTION

Resonant tunneling diodes (RTDs) have extraordinary physical properties[1–3] explored and controlled by the thorough electronic structure engineering that has been attained by modern growth and nano-fabrication techniques. Although fundamentally based on the quantum mechanical tunneling effect, they are devices suitable for room temperature applications[4,5], e.g. RTDs can be found in high frequency oscillators up to the THz regime[6,7], (hot electron) tunneling transistors[8,9] and logic gates[10]. Such richness emerges from a low dimensional and typically just a few nm thick active region in combination with the region of negative differential conductance. This makes RTDs suitable for integrated circuits with reduced circuit complexity, low power consumption and high-speed operation. On the other hand, RTDs are also suitable for electro-optical uses as efficient light detectors[11] and light emitters[12]. Also, they can serve as drivers for semiconductor laser to form a simple optoelectronic integrated circuit (OEIC), a novel alternative to traditional transistor based driver circuits.[13] Usually, to make the charge carrier conductance concur with light emission, bipolar (p-i-n) RTDs are fabricated in which electroluminescence (EL) occurs by electron-hole recombination due to charges injected from differently doped contact layers to the active quantum well region[12,14,15]. However, as reinforced in this paper it is also possible to use unipolar RTDs for this purpose, such as purely n-doped RTDs, where e.g. impact ionization triggered holes are created[16] or via direct tunnelling of carriers from the valence band[17]. In this case, understanding the process of light generation and its correlation with the way the carriers are transported and scattered, becomes a relevant topic to tackle. Yet, the nature of these effects is scarcely investigated since externally tunable parameters with large impact in the system response, such as the position of the resonant voltage, are usually lacking. This is not the case of the RTD used for the present study where the resonant condition can be systematically tuned with temperature and shifted by several Volts. This allows accessing a richer variety of conduction and light emission states with contrasting behaviors.

The thermometric abilities of the RTD, object of the present study, have been characterized in Ref. 4. There, the device electronic structure and the transport response were analyzed in detail. Now, in this paper, we characterize its peculiar EL and discuss the interplay of the various processes involved during light generation. Being a purely n-doped structure, we are able to show that the optical emission originates from impact ionization and a subsequent radiative recombination. We observe that the RTD current and EL intensity are both bistable, yet their respective high and low states can be either inverted, at higher temperatures, or tuned to direct when the temperature is reduced. The emergence of intrinsic bistabilities in the EL has been reported in bi-polar p-i-n RTDs.[12,15,18] Most of these studies report direct correlation between the current and the EL intensity. Yet, inverted and direct bistabilities may coexist as well, as e.g. in triple barrier systems.[19] Unlike our results, the bistabilities reported in Ref. 19 were detected in two different recombination channels involving majority carriers, in the case of the direct bistability, and minority

ones, for the inverted bistability, with the contribution of carriers that remained after the main recombination took place in the multibarrier structure. We propose in this paper a concise explanation for the tuning of direct to inverted EL bistability in the same emission channel produced by impact ionization in unipolar RTDs.

Although counterintuitive, the main effects shown here are obtained by reinforcing undesirable RTDs properties: enhancing the resonant voltage and lowering the peak-to-valley current ratio. Usually for high frequency and low power operations, the enhancement of the peak-to-valley current ratio and the reduction of the resonance voltage are paramount[20]. Lowering the resonance voltage, e.g. via prewell injection and optimization of the doping and heterostructures profile, enables a reduction of the power consumption that allows energy efficient operation of RTDs. High peak-to-valley current ratios on the other hand are required for logic operations (high on/off ratio) as well as for high output powers of RTD GHz oscillators.[21] In contrast, we will explain the seeming paradox of enhancing the on/off ratio of the luminescence with the temperature increase. The correlation of the electronic structure, scattering processes, and ionization mechanisms will be presented and discussed in the paper starting in Section II with the description of the device layout and the room temperature characterization of its optical response. In Section III we discuss the temperature tuning of the light emission and Section IV summarizes the results and draws the conclusions.

II. DEVICE LAYOUT AND ROOM TEMPERATURE EL-EMISSION

Fig. 1(a) shows a sketch of the RTD device layout. The RTDs are grown by molecular beam epitaxy on a silicon n-doped (100) GaAs substrate with doping concentration of $3 \cdot 10^{18}$ cm^{-3}. On top, 300 nm GaAs with a decreasing doping concentration from $1 \cdot 10^{18}$ cm^{-3} to $1 \cdot 10^{17}$ cm^{-3} and the undoped double barrier structure (DBS) are grown. The DBS consists of 15 nm GaAs, 3 nm $Al_{0.6}Ga_{0.4}As$, 4 nm GaAs, 3 nm $Al_{0.6}Ga_{0.4}As$, 5 nm GaAs and 10 nm GaInNAs layers. The growth process is finalized by a 154 nm thick GaInNAs layer with $1 \cdot 10^{17}$ cm^{-3} and by an extended GaAs collector region with a thickness of 556 nm and doping concentration $1 \cdot 10^{18}$ cm^{-3}. The GaInNAs layer is grown latticed matched to GaAs with a bandgap energy of $E_g = 0.95$ eV which enables the RTD to be operated as sensitive photo-detector for telecommunication wavelengths[22,23]. Additionally, it ensures a linear tuning of the resonance voltage with temperature over a broad temperature range[4]. Electron beam lithography and dry chemical etching techniques are used to define RTD mesas with diameters from $d = 12$ to 1 μm. The bottom emitter contact is formed by alloyed AuGe/Ni/Au and an Ti/Au ring-shaped contact is deposited on top of the mesa.

A typical current-voltage characteristic of an RTD

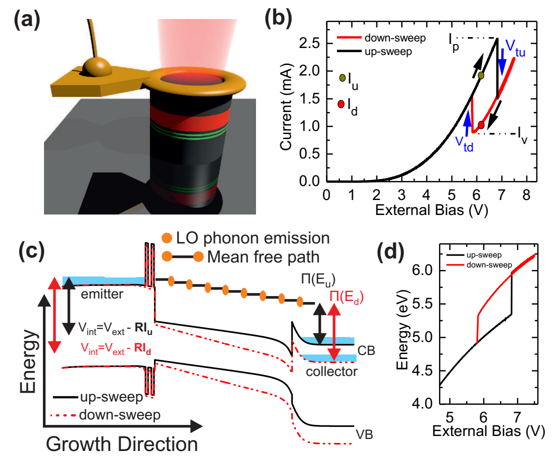

FIG. 1: (a) Sketch of the device layout with the double barrier structure (green) and the GaInNAs drift region (red). On top, an Au ring shaped contact provides the electrial contact in combination with an optical window. (b) RTD current-voltage characteristic at $T = 300$ K, with threshold voltages V_{tu} and V_{td} for the up- and down-sweep direction, respectively. (c) Self-consistent calculation of the conduction (CB) and valence band (VB) profile with currents I_u and I_d (see (b)), and an identical externally applied bias voltage V_{ext}. (d) Injected electron energy between the up- and down sweep direction versus the external bias.

mesa with diameter $d = 5$ μm, recorded at $T = 300$ K, is plotted in Fig. 1(b). The RTD is bistable with a peak current of $I_p = 2.6$ mA, a valley current of $I_v = 0.9$ mA, a peak-to-valley current ratio $PVR_{cur} = I_p/I_v = 2.9$, and threshold voltages $V_{tu} = 6.83$ V for the up- and $V_{td} = 5.86$ V for the down-sweep directions, respectively. The bistable RTD current-voltage characteristic originates from its negative differential conductance region in combination with a series load resistance. The total load resistance R is the sum of the extrinsic load resistance, $R_e = 10$ Ω, and additional parasitic resistances, R_p, with $R = R_e + R_p$[20]. The value of the load resistance can be estimated from the width of the bistable region and the peak and valley currents with $R \sim (V_{tu} - V_{td})/(I_p - I_v) \sim 570$ Ω. Fig. 1(c) shows simulated self-consistent solutions of the valence (VB) and conduction band (CB) profiles associated with two tunneling conditions within the bistable region. The currents are I_u and I_d, but the externally applied bias voltage (V_{ext}) is identical. The internal voltage drop (V_{int}) however differs and, subsequently, the energy of injected electrons in the collector region, $E = q \cdot V_{int}$ (q denotes the elementary charge). With $V_{int}(I) = V_{ext} - R \cdot I$, the energy difference between the up- and down-sweep direction can thus be estimated as $\Delta E = q \cdot [V_{int}(I_u) - V_{int}(I_d)] = q \cdot R(I_u - I_d)$, which for the situation depicted in Fig. 1(b) is about 513 meV. Fig. 1(d) shows the calculated injected electron energy as a function of the external bias voltage. Within the bistable region, the electron energy for the down-sweep direction is enhanced compared to the up-sweep direction.

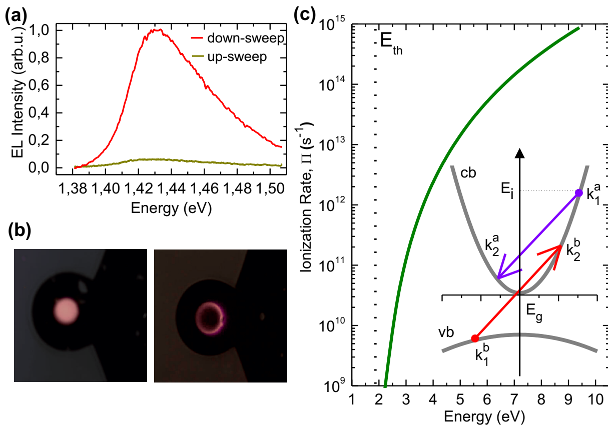

FIG. 2: (a) EL spectra recorded in the up- and down-sweep direction with $V_{\rm ext} = 6.2$ V (see dots in Fig. 1(b)). (b) Optical microscopy images of the RTD contact and EL signal of the non-etched sample (left) and the collector-etched sample (right). (c) Calculated impact ionization rate as a function of the incident electron energy. The inset shows the energy and momentum conservation of the inter- and intra-subband transitions involved in the impact ionization process.

Fig. 2(a) shows two EL spectra, both recorded at $V_{\rm ext} = 6.2$ V (see Fig. 1(b)), but once for the down- and once for the up-sweep direction with currents $I_{\rm d} = 1.0$ mA and $I_{\rm u} = 1.9$ mA, respectively. The EL intensity for the down-sweep direction $EL_{\rm d} = EL(I_{\rm d})$ is significantly enhanced compared to the EL intensity for the up-sweep direction $EL_{\rm u} = EL(I_{\rm u})$, although $I_{\rm u} > I_{\rm d}$. Note that the energy of the EL maximum corresponds to the energy of the GaAs band edge, E_g(GaAs). Hence, to determine the spatial origin of the EL emission, whether from the emitter or collector regions, we compare the sample with a RTD mesa for which most parts of the extended collector GaAs region are removed by dry chemical etching. Here, the ring-shaped top contact is used as etching mask. A central trench with a depth of around 400 nm is etched in the RTD mesa, which leaves about 150 nm GaAs on top of the GaInNAs layer. Fig. 2(b) shows two optical microscope images of the ring-shaped contacts of both, the non-etched sample (left) and the collector-etched sample (right). Then, by biasing both RTDs in a regime when the EL occurs, i.e. $V_{\rm ext} > V_{\rm tu}$, two distinct emission patterns of the two mesas can be observed. An almost uniform EL emission (bright spot) is found for the non-etched sample. In contrast for the collector-etched sample, the EL intensity is reduced significantly and originates only at the outer part close to the ring shaped Au-contacts. This leads to the conclusion that the EL mainly originates from the collector (closer to the contact) and not from the emitter region of the tunneling device.

In fact, the collector region as well as the whole structure is purely n-doped. Thus, the only available process for hole generation in the valence band is the impact ionization. By using the generalized Keldysh model, described in Ref. 24, the hole generation probability can be characterized by the ionization rate, calculated as[25]

$$\Pi(E) = C\left(\frac{E - E_{\rm th}}{E_{\rm th}}\right)^a, \tag{1}$$

where E is the electron energy, $C = 93.659 \cdot 10^{10}$ s^{-1} and $a = 4.743$ for GaAs[24], and $E_{\rm th}$ is the threshold energy above which the ionization process is triggered. By considering energy and momentum conservation during the inter- and intra-subband transitions involved in the ionization processes, as illustrated in the inset of Fig. 2(c), the value of $E_{\rm th}$ can be obtained as $E_{\rm th} = (1 + 2m_c/m_{hh})(1 + m_c/m_{hh})E_g$, with m_c and m_{hh}, the conduction and heavy-hole band masses, respectively. The calculated ionization rate-energy dependence for bulk GaAs is displayed in Fig. 2(c).

The detailed bias voltage dependence of the integrated EL intensity (open circles) and the corresponding RTD current (line), both recorded at $T = 300$ K, are plotted in Fig. 3(a). For the up-sweep direction, the EL intensity increases slightly from $V_{\rm ext} = 5.20$ to 5.84 V. When passing the threshold voltage, $V_{\rm tu} = 5.84$ V, a steep jump of the EL intensity occurs and remains high as the voltage grows. On the contrary, for the down-sweep direction a steep drop of the EL intensity occurs by passing the threshold voltage, $V_{\rm td} = 5.72$ V. Thus under these conditions, the EL emission is bistable within the bias voltage range $V_{\rm td} < V_{\rm ext} < V_{\rm tu}$, but inverted with respect to the current of the tunneling device. Hence, the electrical off-state (low current) corresponds to an optical on-state (high intensity) and vice-versa with the EL emission on/off ratio, $EL_{\rm d}/EL_{\rm u} = 14$, exceeding the electrical peak-to-valley current ratio, $PVR_{\rm cur} = 2.3$, by a factor of 6.

A priori, the EL emission on/off ratio seems disconnected from the current and the electron accumulation densities at the emitter side of the tunneling device which would cause a non-inverted EL signal[26]. To explain this counterintuitive EL-current response we start by calculating the impact ionization rate as a function of the electron energy. First, we assume that the energy of electrons that trigger the impact ionization process in the extended collector region, and hence create holes which radiatively recombine and generate the detected EL signal, is $E = qV_{\rm int} - E_{los}$. Here, $V_{\rm int}$ is the internal voltage drop the electrons undergo after leaving the DBS towards the collector and can be related to the externally applied bias. The energy loss term, E_{los}, accounts for different energy loss mechanisms such as LO-phonon emission events (see Fig. 1(c)), impact ionization processes in the GaInNAs region, and additional parasitic voltage drops. For polar GaAs and the high energy electrons involved in the ionization process, the energy loss is mainly attributed to LO-phonon generation (see Reference[27] for a discussion about optical and acoustic phonon contributions) with an energy loss of 36 meV per phonon emission[28,29].

Fig. 3(b) displays the calculated impact ionization rate

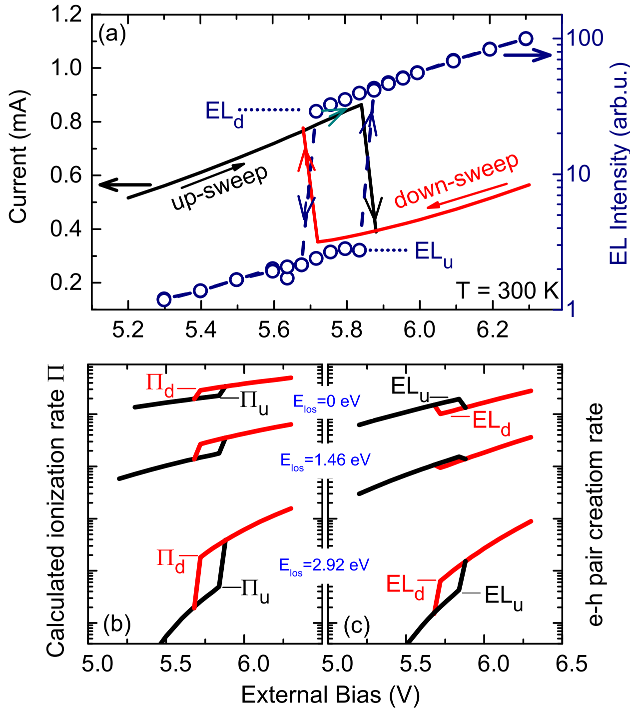

FIG. 3: (a) RTD current-voltage characteristic (line) and integrated EL intensity (open circle) for the up- and the down-sweep direction. For the up-sweep direction, the EL intensity increases significantly when passing the threshold voltage $V_{\rm tu}$ and drops for the down-sweep direction when passing $V_{\rm td}$. The EL intensity is bistable with an on/off ratio of 14 and its intensity is inverted with respect to the current within the threshold voltages $V_{\rm tu}$ and $V_{\rm td}$. (b) Calculated ionization rate, Π, as a function of the external bias for different E_{los} from 0 to 2.92 eV. (c) Calculated electron-hole pair generation rate as a function of the external bias for different E_{los} from 0 to 2.92 eV.

Π as a function of the external bias voltage for different E_{los}. By ascribing the whole energy loss mechanism to the LO-phonons emission, this would correspond to $n = 0$, 40, and 80 scattering events for $E_{los} = 0$, 1.46 and 2.92 eV, respectively. One should note however that these values are overestimated since, as stated before, parasitic voltage drops that also contribute to E_{los} are embedded along the RTD band profile. Yet, they could not be accounted for accurately within the self-consistent model which results are shown in Fig. 1(c). One observes that the impact ionization rate is always larger for the down-sweep direction compared to the up-sweep direction and it shows an inverted bistability analogous to the EL emission presented in Fig. 3(a). This can be understood as follows: within the bistable region and for electrons arriving at the collector above the ionization threshold ($qV_{\rm ext} - qRI - E_{los} > E_{\rm th}$), the ratio of the ionization rates at the down-sweep direction, $\Pi_{\rm d} = \Pi(qV_{\rm ext} - qRI_{\rm d} - E_{los})$, and up-sweep direction, $\Pi_{\rm u} = \Pi(qV_{\rm ext} - qRI_{\rm u} - E_{los})$ is given, according to Eq. 1, by

$$\frac{\Pi_{\rm d}}{\Pi_{\rm u}} = \left(1 + \frac{qR \cdot (I_{\rm u} - I_{\rm d})}{qV_{\rm ext} - qR \cdot I_{\rm u} - E_{los} - E_{\rm th}}\right)^a. \quad (2)$$

Thus for $I_{\rm u} > I_{\rm d}$, then inevitably, $\Pi_{\rm d}/\Pi_{\rm u} > 1$. According to Eq. 2, the value of the ratio $\Pi_{\rm d}/\Pi_{\rm u}$ increases as E_{los} grows (see Fig. 3(b)). For a constant E_{los}, an analogous effect would be obtained by decreasing the resonance voltage.

In the next section, we will return to this peculiar behavior that accounts for the increase of the on/off resolution with temperature. Before that, we shall acknowledge that the EL intensity does not solely depend on the net ionization probability; it is also proportional to the current. Obviously, only a fraction η of the current accounts for the detected EL signal, since e.g. thermalized electrons or electrons with energies below $E_{\rm th}$ will not trigger an impact ionization process at the collector side. Thus, to complete the picture of the electron-hole (e-h) pair generation one must analyze the evolution of $EL(V_{\rm ext}) = \Pi(V_{\rm ext}) \cdot \eta \cdot I(V_{\rm ext})$, which is displayed in Fig. 3(c).

For large E_{los} values, the bistable e-h generation follows the experimental trend of Fig. 3(a) ($EL_{\rm d} > EL_{\rm u}$) yet reverses for lower E_{los} ($EL_{\rm d} < EL_{\rm u}$). According to Eq. 2, analogous affects would be obtained by increasing the external bias at resonance, $V_{\rm res} = V_{\rm ext}(I_{\rm p})$. Thus, without losses ($E_{los} = 0$), for a resonance voltage of about 5.9 V and a $PVR_{\rm cur}$ of 2.3, a non-inverted EL intensity-RTD current response would occur. Analogously, keeping constant all other parameters while increasing the $PVR_{\rm cur}$ would narrow the inverted EL intensity ratio attaining a non-inverted response at a certain point. In our case, the interplay of the moderate $PVR_{\rm cur}$, the large resonance voltage, and the energy losses enable the observation of the EL intensity inversion. The EL intensity inversion leads to an electro-optical logic NOT gate operation of the device with an electrical low input (low current) corresponding to an optical high output (high EL intensity) and vice versa. As pointed out previously, this is only achieved by commonly undesired RTD figure-of-merits: large resonant voltages (to account for impact ionization processes to occur) and moderate peak-to-valley current ratios (to account for the higher impact ionization rate for the valley region). Combining the functionalities of the device being a light emitter and light sensor within the same bias voltage range[22] potentially enable all-optical logic operation.

Thus, according to this model, the ratio $\frac{EL_{\rm d}}{EL_{\rm u}} = \frac{\Pi_{\rm d}}{\Pi_{\rm u}} \cdot \frac{I_{\rm d}}{I_{\rm u}}$ can either be larger or smaller than 1 by tuning $\frac{\Pi_{\rm d}}{\Pi_{\rm u}}$, since $\frac{I_{\rm d}}{I_{\rm u}} < 1$ and is almost unchanged under any circumstances. For a constant $\frac{I_{\rm d}}{I_{\rm u}}$ ratio and E_{los}, a process for which $\frac{EL_{\rm d}}{EL_{\rm u}} < 1$ occurs would be available for higher incoming electron energies, i.e higher resonance voltages. These conditions can be experimentally attained in our RTD and will be described in the next section.

III. TEMPERATURE TUNING OF THE EL-EMISSION

Fig. 4(a) shows RTD current-voltage characteristics and the corresponding normalized integrated EL intensities (b) for temperatures between $T = 300$ and 60 K. As the temperature is reduced, the peak position of the EL emission shifts to higher energies and coincided with the expected spectral position at the measured environmental temperature.[4] From fitting the low energy side of the spectrum, a heating of the sample with around 50 K above the base temperature is observed that is however constant over the whole temperature and current range and hence just provides a constant background.

The temperature reduction shifts the electron resonance of the RTD towards higher external voltages and, simultaneously, the EL bistable states narrow their on/off ratio. Here, we utilize the capability of our device of shifting the RTD threshold voltages, $V_{\rm tu}$ and $V_{\rm td}$, to larger external bias values by reducing the temperature, as described in Ref. 4. This effect originates at the junction between the GaInNAs layer and the n-doped GaAs region where a temperature dependent sheet density induces an additional screening field. Thus, the absolute value of the external bias needed to attain the resonant voltage at the double barrier grows with decreasing temperature, increasing in turn the injected electron energy in the collector region. Over the whole temperature range, the EL and RTD bistability is evident. More important yet, the on/off states of the EL weakens and even invert their relative positions below $T = 100$ K. We should note that the results illustrated in Fig. 4(b) were normalized to the maximum intensity to provide a better picture of the relative shift between $EL_{\rm u}$ and $EL_{\rm d}$. Yet, as expected from Eq. 1 and Fig. 2(c), the absolute values of the ionization rate are reduced with decreasing energy of the incoming electrons. This can be corroborated in the reduction of the absolute EL intensity with increasing temperature.

For a better characterization of the EL ratio tuning with temperature, the peak-to-valley current ratios and EL emission ratio, $\frac{EL_{\rm d}}{EL_{\rm u}}$, are plotted in Fig. 5(a). The electrical $PVR_{\rm cur}$ is almost constant over the temperature range from $T = 300$ to 60 K. In contrast, the optical ratio shrinks when the temperature is reduced and even inverts for $T = 60$ K with $\frac{EL_{\rm d}}{EL_{\rm u}} < 1$. Under these conditions, Eq. 2 indicates that the hole generation rate will be predominantly controlled by the difference, $qV_{\rm ext} - E_{los}$. The experimentally obtained impact ionization rate versus internal bias, $\Pi(V_{\rm int})$, is calculated from the I(V) curves and the EL intensity, $\Pi(V_{\rm int}) \propto \frac{EL(V_{\rm int})}{I(V_{\rm int})}$. $\Pi(V_{\rm int})$ is plotted in Fig. 5(b) for the EL signals shown in Fig. 4(a) (current) and (b) (EL). Since the peak and valley currents remain almost constant over the temperature range (as shown in Fig. 4(a)), the ionization rate (as depicted in Fig. 5(b)) is directly proportional to the absolute EL intensity which increases exponentially as the temperature is reduced. The calculated impact ionization rates according to Eq. 1 with $E_{los} = 2.70$ eV

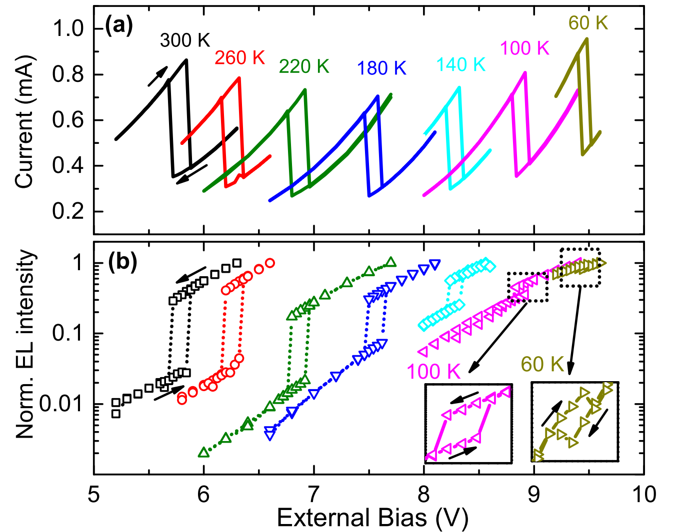

FIG. 4: RTD current (a) and normalized integrated EL intensity (b) versus the external bias voltage for temperatures ranging from $T = 300$ to 60 K. The insets in panel (b) show the details of the integrated EL intensity near resonance for $T = 100$ and 60 K.

(renormalization of the threshold energy) provide a good agreement with the experiment.

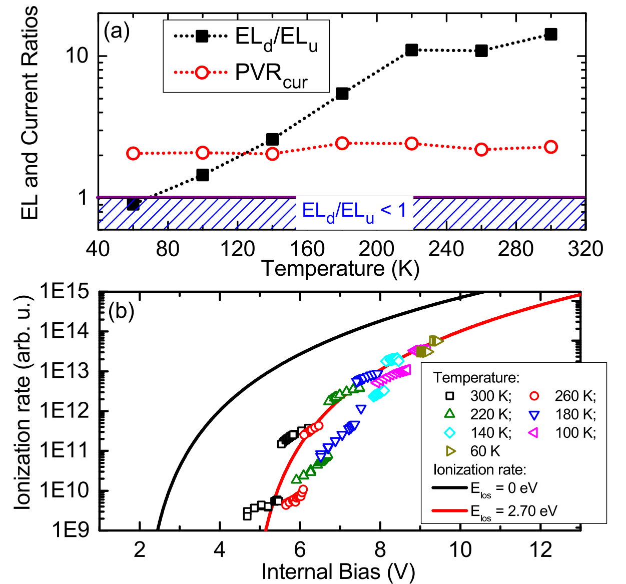

FIG. 5: (a) Temperature dependence of the experimental electrical peak-to-valley current ratios $PVR_{\rm cur}$ and the EL emission ratio. (b) Comparison between the theoretical and calculated impact ionization. Without E_{los}, the ionization rate increases as soon as the threshold E_{th} is surpassed. A good agreement between theory and experiment can be evaluated via $E_{los} = 2.70$ eV.

IV. CONCLUSION

In summary, we built and characterized a device that tunes the bistable EL emission of purely n-doped AlGaAs/GaAs double barrier resonant tunneling diodes. Enhanced on/off resolution of the optical emission can be attained at room or higher temperatures. Based on these results, it is possible to conclude that the EL originates from impact ionization and radiative recombination in the collector region of the tunneling device and, in the bistable current condition, the emission occurs for low and vanishes for high tunneling currents in a wide temperature range. The EL bistability can be both inverted or not with respect to the tunneling current density according to temperature values. In this process, two conflicting parameters concur: the amount of incoming electrons, proportional to the current, and the ionization probability that depends on the incoming energy. Both depend on the conduction states that were accessible, in this case, thanks to the peculiar thermometric response of the studied RTD. We should note that the highest optical on/off ratio of 14 has been attained at room temperature which exceeds the current on/off ratio by a factor of 6.

Acknowledgments

The authors are grateful for financial support by the BMBF via national project EIPHRIK (FKZ: 13N10710), the European Union (FPVII (2007-2013) under grant agreement no. 318287 LANDAUER), and the Brazilian Agencies CNPq and CAPES. S. H. gratefully acknowledges support by the Royal Society and the Wolfson Foundation. Expert technical assistance by M. Emmerling and S. Handel is gratefully acknowledged.

[1] R. Tsu and L. Esaki, Appl. Phys. Lett. **22**, 562 (1973).
[2] H. B. de Carvalho, Y. Galvao Gobato, M. J. S. P. Brasil, V. Lopez-Richard, G. E. Marques, I. Camps, M. Henini, L. Eaves, and G. Hill, Phys. Rev. B **73**, 155317 (2006).
[3] H. B. de Carvalho, M. J. S. P. Brasil, V. Lopez-Richard, Y. Galvao Gobato, G. E. Marques, I. Camps, L. C. O. Dacal, M. Henini, L. Eaves, and G. Hill, Phys. Rev. B **74**, 041305R (2006).
[4] A. Pfenning, F. Hartmann, M. Rebello Sousa Dias, L. K. Castelano, C. Süßmeier, F. Langer, S. Höfling, M. Kamp, G. E. Marques, L. Worschech, V. Lopez-Richard, ACS Nano **9**, 6271 (2015).
[5] S. Suzuki, M. Asada, A. Teranishi, H. Sugiyama, and H. Yokoyama, Appl. Phys. Lett. **97**, 242102 (2010).
[6] M. Asada, and S. Suzuki, IEEE Photonic Tech. L. **8**, 1110 (2011).
[7] M. Feiginov, H. Kanaya, S. Suzuki, and M. Asada, Appl. Phys. Lett. **104**, 243509 (2014).
[8] F. Capasso, R. Kiehl, J. Appl. Phys., **58**, 1366-1368, (1985).
[9] G. I. Haddad, U. K. Reddy, J. P. Sun, and R. K. Mains, Superlattices Microstruct. **7**, 369-374, (1990).
[10] Y. Zheng, and C. Huang, IEEE T. Nanotechnol. **8**, 631 (2009).
[11] J. Blakesley, P. See, A. Shields, B. Kardyna, P. Atkinson, I. Farrer, and D. Ritchie, Phys. Rev. Lett. **94** 067401 (2005).
[12] S. M. Cao, M. Willander, A. A. Toropov, T. V. Shubina, B. Ya. Meltser, P. S. Kopev, T. Lundström, P. O. Holtz, J. P. Bergman, and B. Monemar, Appl. Phys. Lett. **72**, 347 (1998).
[13] T. J. Slight, and C.N. Ironside, IEEE J. Quantum Elect. **43**, 580 (2007).
[14] R. Teissier, J. W. Cockburn, P. D. Buckle, M. S. Skolnick, J. J. Finley, R. Grey, G. Hill, and M. A. Pate, Phys. Rev. B **50**, 4885 (1994).
[15] C. Van Hoof, J. Genoe, R. Mertens, G. Borghs, and E. Goovaerts, Appl. Phys. Lett. **60**, 77 (1992).
[16] C. R. H. White, L. Eaves, M. L. Leadbeater, M. Henini, D. H. Hughes, G. Hill, and N. A. Pate, Superlattice Microst. **8**, 391 (1990).
[17] C.-S. Lin, K. Cavanagh, H.-C. L. Tsui, A. Mihai, B. Zou, D. W.E. Allsopp, and M. A. Moram, IEEE Photonics Journal **9**, 2201008 (2017).
[18] C. Van Hoof, J. Genoe, R. Mertens, G. Borghs, and E. Goovaerts, Electronics Letters **28**, 123 (1992).
[19] P. A. Harrison, L. Eaves , P. M. Martin , M. Henini , P.D. Buckle, M. S. Skolnick, D. M. Whittaker, G. Hill, Surface Science **305**, 353 (1994)
[20] H. Mizuta and T. Tanoue, “The Physics and Applications of Resonant Tunnelling Diodes”, ed. Cambridge University Press (1995).
[21] J. Wang, L. Wang, C. Li, and E. Wasige, Electronics Letters **49**, 816-818 (2013).
[22] F. Hartmann, F. Langer, D. Bisping, A. Musterer, S. Höfling, M. Kamp, A. Forchel, and L. Worschech, Appl. Phys. Lett. **100**, 172113 (2012).
[23] A. Pfenning, F. Hartmann, F. Langer, S. Höfling, M. Kamp and L. Worschech, Appl. Phys. Lett. **104**, 101109 (2014).
[24] R. Redmer, J. R. Madureira, N. Fitzer, S. M. Goodnick, W. Schattke, and E. Scholl, J. Appl. Phys. **87**, 781 (2000).
[25] L. V. Keldysh, Zh. Eksp. Teor. Fiz. **37**, 713 (1959) [Sov. Phys. JETP **37**, 509 (1960)].
[26] C. R. H. White, M. S. Skolnick, L. Eaves, and M. L. Leadbeater, Appl. Phys. Lett. **58**, 1164 (1991).
[27] M. Bernardi, D. Vigil-Fowler, C. Shen Ong, J. B. Neaton, and S. G. Louiea, PNAS **112**, 52915296 (2015).
[28] H. Fröhlich, Adv. in Phys. **3**, 325 (1954).
[29] H. Shichijo and K. Hess, Phys. Rev. B **23**, 4197 (1981).